Negative pion-nucleus elastic scattering at 30 and 50 MeV

Kamal K. Seth, D. Barlow,* S. Iversen,† M. Kaletka,‡ H. Nann,§ D. Smith, and M. Artuso**
Northwestern University, Evanston, Illinois 60208

G. Burleson, G. Blanpied,†† and G. Daw‡‡
New Mexico State University, Las Cruces, New Mexico 88003

W. J. Burger§§ and R. P. Redwine
Massachusetts Institute of Technology, Cambridge, Massachusetts 02139

B. Saghai
CEN de Saclay, 91191 Gif-sur-Yvette, France

R. Anderson
Los Alamos National Laboratory, Los Alamos, New Mexico 87545
(Received 29 September 1989)

Differential cross sections for the elastic scattering of 30 and 50 MeV π^- by nuclei ranging from ^{12}C to ^{208}Pb have been measured using a range spectrometer. Comparison is made with the predictions of a recent optical-model calculation and the general nature of discrepancies is discussed.

I. INTRODUCTION

The study of pion elastic scattering from nuclei is an important ingredient in the understanding of pi-nucleus interactions. Without an understanding of elastic scattering it is not possible to address the physics of pion charge exchange, pion absorption, pion production, and other reactions. Numerous measurements of elastic scattering from nuclei have been made since the earliest days of pion physics. Most such measurements have been made at energies in the vicinity of the $\Delta(3,3)$ resonance, $T(\pi)=200\pm100$ MeV, where the cross sections are large, and the experimental difficulties are minimized. In the $\Delta(3,3)$ energy region the nucleus appears almost "black" to pions, and elastic scattering is dominated by diffractive features. For this reason these measurements do not shed light on many of the interesting aspects of pion-nucleus interactions. To probe the nuclear interior, to delineate the effects of the "polarization" of the nuclear medium (the so-called LLEE, Lorentz-Lorenz-Ericson-Ericson effect), and to make connections with the pionic-atom problem, it is necessary to study the scattering of low-energy pions from nuclei. As one moves to lower energies the pi-nucleon interaction becomes progressively less dominated by the Δ resonance, the nucleus becomes more transparent, and the subtler aspects of the pi-nucleus interaction manifest themselves. During the past ten years several measurements of pion elastic scattering at energies of 50 MeV and lower have been reported.[1-7] However, because of experimental reasons most measurements have been confined to π^+ scattering, and the paucity of experimental data on low-energy π^- elastic scattering has prevented a proper understanding of the isovector (and to some extent, isotensor) component of the pi-nucleus interaction. It is in response to this need that the present set of measurements of π^- elastic scattering was made.

II. EXPERIMENTAL DETAILS

One of the main reasons for the sparsity of π^- elastic scattering data is the fact that total energy detecting devices, whether intrinsic germanium detectors[1] or plastic scintillation counters,[2-5] do not lend themselves conveniently to negative pion detection. After its eventual slowing down and capture, the π^- is absorbed, creating a "star." The energy released in this absorption process overwhelms the signal due to the kinetic energy loss by the pion. One way to get around this problem is to use magnetic spectrometers for momentum measurement and ΔE counters for pion detection and identification. Recently several specially designed spectrometers with large solid angles were commissioned, and the first π^- scattering data from these facilities are beginning to appear.[6,7] A different technique is to replace the total energy measurement by the range measurement in a segmented range spectrometer. This very old technique[8] was recently successfully revived at Saclay[9] for precision measurements of low-energy $\pi^- p$, $\pi^- d$, and $\pi^{-\,3,4}$He cross sections. Following on the experience at Saclay, we have designed and constructed a 24-segment range spectrometer and successfully used it to make the measurements reported here.

The measurements were made at the low-energy pion (LEP) channel of the Clinton P. Anderson Meson Physics Facility (LAMPF) at the Los Alamos National Laboratory. Pion beams of 30- and 50-MeV energy were used with a momentum spread $\Delta p/p=\pm1\%$. The beam spot size

was measured by means of a current-integrating wire chamber and found to be ~ 3.8 cm (H)$\times 1.2$ cm (V). The usable π^- flux was $\sim 8\times 10^6$ π^-/sec at 50 MeV and $\sim 1.7\times 10^6$ π^-/sec at 30 MeV.

The floor plan of the experimental setup is shown in Fig. 1. The scattering target was located about one meter from the exit port of the LEP channel. The entire spectrometer system, containing all detectors except the decay muon beam monitor, rotated about this point in the angular range 0° to 145°.

The pion intensity was monitored with a two-element scintillator counter telescope[10] (decay muon monitor) placed at 10° to the incident beam, as shown in Fig. 1. This telescope identified and counted muons from the decay of beam pions. It was periodically calibrated against a direct measurement of the number of pions in the beam. This was done by means of a scintillator telescope placed in the pion beam while the primary proton beam intensity was reduced by factor ~ 100.

The scattering targets were all generously larger than the beam-spot size. The thicknesses, enrichments, and energies of the first excited states of the targets are listed in Table I. The ^{16}O target was in the form of a gel: water with $\sim 1.5\%$ agar. It was enclosed in mylar foils of $\frac{1}{2}$-ml thickness. All other targets were in the form of self-supporting foils.

As schematically illustrated in Fig. 1, the complete spectrometer system consisted of 32 counters. As seen by the scattered beam these were (distances z measured from target) the following:

(a) T, a scintillation counter to define events originating in the target, $7.62\times 7.62\times 0.32$ cm ($z=13$ cm).

(b) $F1$–3, three (finger) scintillation counters to define solid angles at $\theta=\theta_0-5°$, $\theta=\theta_0$, and $\theta=\theta_0+5°$, each counter $2.54\times 7.62\times 0.32$ cm [$z=46.2$ cm (50 MeV), $z=44.0$ cm (30 MeV)]. Each scintillator subtended $\sim\pm 1.8°$ at the target.

(c) $\check{C}1$, $\check{C}2$, two Lucite Čerenkov counters to identify electrons and positrons, each counter $20.3\times 20.3\times 1.27$ cm ($z=47$–49 cm).

(d) $S1$–$S24$, 24 scintillation counters to determine range, each 15.2×15.2 cm, with thicknesses $S1$–$S4$ and $S21$–$S24$, each 0.635 cm, $S5$–$S8$ and $S17$–$S20$, each 0.254 cm, $S9$–$S16$, each 0.126 cm ($z=51$–75 cm).

(e) $V1$, $V2$, two scintillation counters flanking the detector stack in order to allow vetoing those events in which the pions are scattered out of the detector stack, each scintillator $30.5\times 20.3\times 1.27$ cm ($z=50$–80 cm).

In order to have the best possible resolution in range measurement, the range spectrometer was designed to have a "coarse grain" (large differential range steps) at the beginning as well as at the end, and to have a fine grain (small differential range steps) in the vicinity of the Bragg edge. The total material in the path of the pions was increased (by adding Lucite absorbers between the $\check{C}2$ and $S1$ counters) or decreased (by removing absorbers and thick counters) in order to arrange for elastically scattered pions to stop near the center of the fine-grain region (counter $S12$–13). The gains of the counters were balanced with e^+ in the π^+ beam, as identified by the Čerenkov counters.

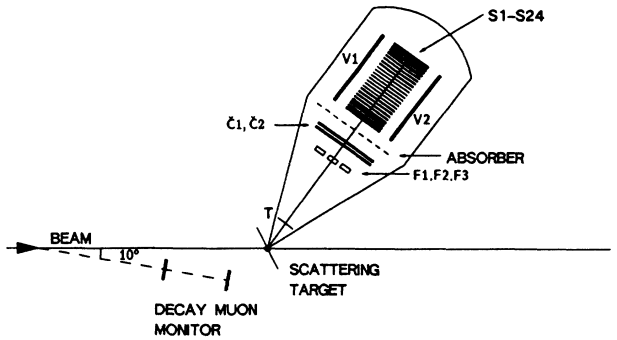

FIG. 1. Schematic illustration of the floor plan of the experimental setup.

Scattering measurements were made in two different geometries. For $\theta\leq 90°$, a transmission geometry was used, with the target rotated at an angle θ(target)$=\theta$(scatt.)/2. For $\theta\geq 90°$, a reflection geometry was used, with θ(target)$=90°+\theta$(scatt.)/2. At 90° measurements were made in both geometries and found to agree within the quoted uncertainties.

For incident pion energy of 50 MeV, the full complement of detectors plus a Lucite absorber (1.27–1.59-cm thick) were used. The hardware event trigger was defined as

$$T\cdot(F1 \text{ or } F2 \text{ or } F3)\cdot S1\cdot S2\cdot S3\cdot S4\cdot(\overline{\check{C}1}\cdot\overline{\check{C}2}) ,$$

i.e., it was required that the particle must originate in the target area, it must traverse one of the three finger counters, and it must not stop in counters $S1$–3. It must also not be registered as an electron in the Čerenkov counters. The electron efficiency of the Čerenkov veto was only $\sim 50\%$, so that the trigger also included some electron events. For 30-MeV measurements $\check{C}1$, $\check{C}2$, and $S3$–6 were removed, an absorber of 1.59-cm thickness was inserted, and the hardware trigger was

$$T\cdot(F1 \text{ or } F2 \text{ or } F3)\cdot S1\cdot S2\cdot S7 .$$

For each trigger, pulse height and logical information were read into an on-line PDP-11/45 computer and recorded on tape. At periodic intervals, scalar information about the primary proton beam, the decay muon monitor, singles in various counters, and coincidences

TABLE I. Enrichments, thicknesses, and first excited states of the targets used.

Target	Enrichment	Thickness (mg/cm^2)	E^* (J^π) (MeV)
^{12}C	(natural)	225.8	4.44 (2^+)
^{13}C	99%	206.0	3.09 ($\frac{1}{2}^+$)
^{16}O	(natural)	393.0	6.05 (0^+)
^{40}Ca	(natural)	245.0	3.35 (0^+)
^{48}Ca	94.6%	202.0	3.83 (2^+)
^{90}Zr	96.7%	69.0	1.76 (0^+)
^{208}Pb	98.7%	153.6	2.61 (3^-)

and accidentals were also read in and recorded. A fraction of events was analyzed on line, and pulse height spectra, range histograms, and two-dimensional plots for these were made available during the data collection.

Measurements were made at 10° intervals from 40° to 140° for all targets except ^{208}Pb. For 50 MeV π^- scattering from ^{208}Pb measurements were made at 5° intervals. Several target-out measurements were also made to study background characteristics. At 50 MeV π^+ elastic scattering data were also taken for the targets of ^{12}C, ^{16}O, and ^{208}Pb in order to compare our results with earlier π^+ data obtained with other measuring techniques.[1-6]

III. DATA ANALYSIS

The data accumulated on the tapes were replayed off line to analyze all the events under optimum conditions. The purpose of the analysis was to identify pions in the presence of electrons and muons, and to distinguish the elastic events from all others.

Since the Čerenkov detectors ($\check{C}1$ and $\check{C}2$) were relatively inefficient at 50 MeV and not used at 30 MeV, the triggers in both cases included some electron events. This is illustrated in the typical pulse height spectra for the S counters shown in Fig. 2. The electron and the pion peaks are easily identifiable. The stopping of the pions is clearly seen by the rapidly decreasing area of the pion peak in counters $S10-14$. A good fraction of the electron events could be rejected by requiring a veto with one or more of the last four thick counters ($S21-24$) of the stack, but it was found that this led to rejection of 10–20 % of the true pion events also. No such veto was therefore used, and a "good event" was defined simply as a trigger which was not accompanied by a count in one of the side-escape veto counters $V1$ and $V2$. A "good event" was followed through the counter stack and considered to have stopped in counter $S(n)$ if either no further coincidence was found in counters $S(n+1)$ and $S(n+2)$, or an overflow pulse height (due to "star" formation) was found in $S(n)$. The pulse heights in counters $S(1)\cdots S(n)$ [or $S(1)\cdots S(n-1)$ in case of a "star"] were treated in two different ways to distinguish between electrons and pions. In the first procedure the harmonic mean of pulse heights was constructed as

$$\langle PH\rangle=[PH(1)\times PH(2)\times\cdots\times PH(n)]^{1/n}\ .$$

A typical spectrum of counters vs $\langle PH\rangle$ is shown in Fig. 3. The peak corresponding to the pions is clearly resolved from the e/μ peak on the left. In the second procedure the total energy of the event was reconstructed after carefully calibrating the pulse heights in each detector. The pion elastic peak could then be resolved unambiguously. The summed counts in the pion peaks in the two cases were found to be equivalent. Because of its simplicity the identification by means of the harmonic mean was used for all the data.

For each stopping counter three spectra of the (harmonic) mean pulse heights, corresponding to each of the three finger counters $F1$, $F2$, $F3$, were made. Cuts were made for the pion peak in each spectrum, and the number of "pions" stopping in each counter was plotted as a function of the stopping counter number (or equivalently, as function of range in the scintillator material). Such a plot for the central finger, $F2(\theta=\theta_0)$ is shown in Fig. 4 for π^- scattering from carbon. Similar plots were made for $F1$ and $F2$. In Fig. 4 the elastic peak is clearly identifiable, as is the inelastic peak due to the 4.4-MeV excited state in ^{12}C. The equivalent energy resolution is found to be FWHM ≈ 1.3 MeV. This is quite sufficient to resolve the elastic scattering peaks from inelastic scattering from the first excited states listed in Table I. (The first excited state in ^{90}Zr can be only marginally resolved, but this 0^+ state is known to be very weak.) The counts in the elastic peak $N(\theta,\pi)$ were normalized to

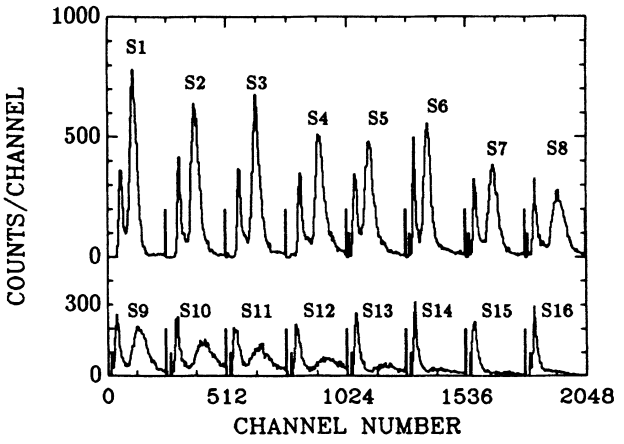

FIG. 2. Pulse height spectra of the first 16 scintillators, $S1-S16$, of the 24-element range spectrometer. The pion "peak" is clearly identifiable. It gradually disappears between detectors $S10$ and $S14$ as the pions are stopped. The spectra are for 50 MeV π^- scattering from ^{12}C at $\theta=120°$.

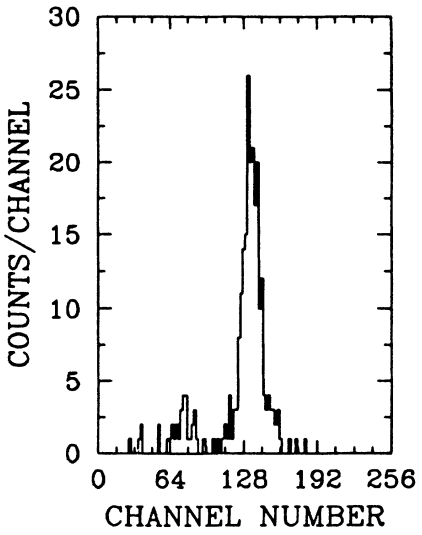

FIG. 3. Harmonic mean of pulse heights for those particles which passed through the center-finger counter F_2 and which stopped in scintillator $S13$. The small peak on the left is due to electrons, the large peak is due to pions. The example is for 50 MeV π^- scattering from ^{12}C at $\theta=120°$.

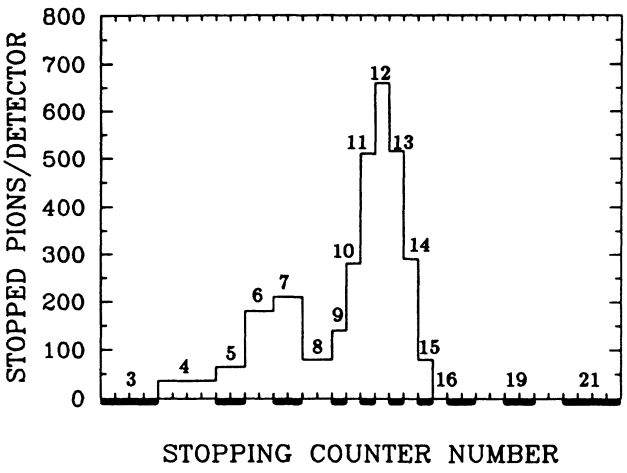

FIG. 4. A typical range spectrum for 50-MeV stopping pions plotted as function of the stopping counter number. The width of the bins shown is proportional to the thickness of the counters.

the muon counts $N(\mu)$ in the monitor to get the relative yields

$$Y(\theta)=N(\theta,\pi)/[N(\mu)\cdot(t/\cos\theta_t)] \ . \quad (1)$$

Here t is the target thickness and θ_t is the target angle. Since data were generally taken with the spectrometer setting every 10°, the two side-finger counters measured scattering at the same angles for two successive settings of the spectrometer. This allowed us to investigate the performance of the side-finger counters $F1$ and $F3$ which were expected to be more sensitive to the outscattering of pions and other edge effects than the central counter $F2$. Indeed, it was found that the yields for $F1$ and $F3$ (when brought to the same angle) were not equal. Further, the differences,

$$\Delta\sigma(\theta)/\langle\sigma(\theta)\rangle \equiv[\sigma(\theta,F3)-\sigma(\theta,F1)]/[\sigma(\theta,F3)+\sigma(\theta,F1)]/2 \quad (2)$$

were found to be systematically angle dependent. They were positive ($+\leq 20\%$) in regions where $\sigma(\theta)$ decreased with increasing angle, negative ($-\leq 15\%$) in regions where $\sigma(\theta)$ increased with angle, and negligibly small in regions where $\sigma(\theta)$ was nearly constant. Monte Carlo calculations provided a qualitative understanding of the $F1/F3$ discrepancies as arising from finite geometry (angular resolution and acceptance) and outscattering from the stack, but quantitative agreement with the magnitude of the effect observed was not achieved. However, both the Monte Carlo calculations and the Pb data (taken ever 5°) indicate that the data from the center-finger counter $F2$ do not suffer from these problems (effect estimated as $<5\%$). Instead of correcting for the $F1/F3$ differences in some empirical manner, it was therefore decided to discard the data from the side counters $F1$ and $F3$. The data presented in this paper are only from the central-finger counter $F2$ at $\theta=\theta_0$. Since the differential cross sections at both 50 and 30 MeV vary slowly with angle, this limitation to 10° angular steps constitutes no serious disadvantage. However, since the angular structure in ^{208}Pb π^- differential cross sections was expected to be more pronounced, these cross sections were measured with the spectrometer set at 5° intervals.

Center-of-mass differential cross sections are related to the yield as

$$d\sigma(\theta)/d\Omega=Y(\theta)J/[R(\pi/\mu)\cdot\Delta\Omega'] \ , \quad (3)$$

where $R(\pi/\mu)$ is the ratio of the number of pions in the beam to the counts in the muon monitor counter. J is the Jacobian relating the laboratory cross sections to those in center of mass, and $\Delta\Omega'$ is the effective laboratory solid angle for the detector system. As already mentioned, values of $R(\pi/\mu)$ were determined by direct measurements in reduced-intensity beams. The effective solid angle $\Delta\Omega'$ differs from the geometrical solid angle $\Delta\Omega$ which was 9.07 msr for the 50-MeV measurements and 10.00 msr for the 30-MeV measurements. The difference between $\Delta\Omega$ and $\Delta\Omega'$ arises due to a loss of the pion flux due to a variety of reasons. These include finite beam dimension and divergence, pion decay, pion scattering out of the stack, multiple Coulomb scattering, pion absorption, and other reactions.

In order to determine the effective solid angle corresponding to our detector system, a Monte Carlo program, which takes account of all inefficiencies (except loss by absorption and other nuclear reactions), was written.[11] This program was based on one written by the Saclay group.[9] The improvements in the present version relate to a more efficient generation of events, a more realistic description of energy loss and straggling (Vavilov distribution as compared to Gaussian), and separate tracking of pions and muons. The output of this program consists of the differential efficiency for each finger counter as a function of the true scattering angle (for a finite size and divergence of the beam) and the stopping counter. This allows the energy spectrum in each counter and the distribution of stopping events in the different counters to be compared with the corresponding experimental distributions. The Monte Carlo program showed that, for the particles which entered the detector stack through the central-finger counter $F2$, beam divergence, nonuniform illumination of the finger, multiple Coulomb scattering, and small misalignments of the detectors did not produce any significant departures of the efficiency from the geometrical one; pion decay and loss due to absorption and reactions in the stack were the main effects. However, for particles through the side fingers, $F1$ and $F3$, beam divergence, nonuniform illumination, multiple Coulomb scattering, and geometrical misalignments were also found to be quite important. Because of the exaggerated sensitivity to these effects the effective solid angles for the side counters could not be obtained reliably. The investigation of this problem was not pursued further because, as already mentioned, it had been decided for other reasons to discard the data for the side fingers and to use only the central-finger data. The effect of pion loss due to absorption and reactions in the detector stack could not be incorporated in the Monte Carlo program

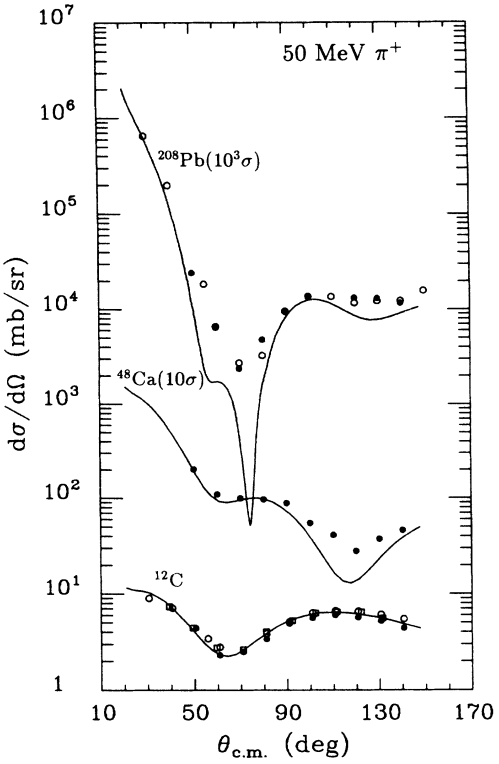

FIG. 5. Center-of-mass differential cross sections for elastic scattering of 50 MeV π^+ from ^{12}C, ^{48}Ca, and ^{208}Pb. The filled circles are results from the present experiment. The open circles are from Ref. 5 and the open squares are from Ref. 6. The statistical errors for all data are smaller than the size of the symbols. The curves are from the optical-model calculations of Siciliano *et al.* (Ref. 17).

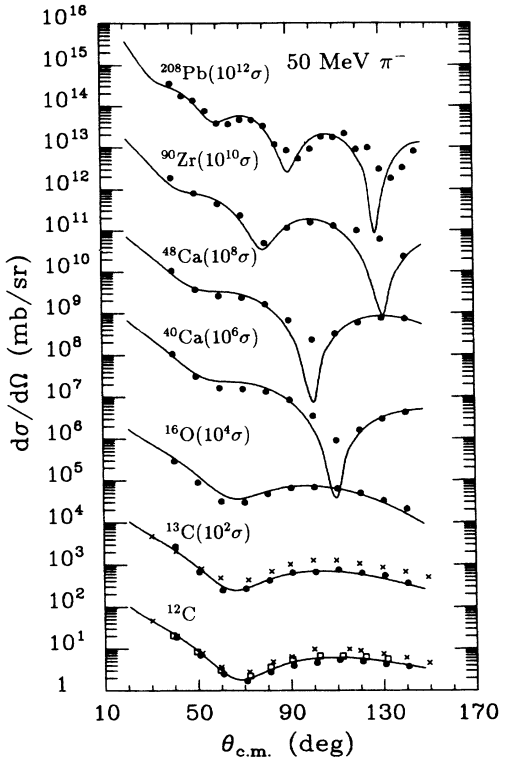

FIG. 6. Center-of-mass differential cross sections for elastic scattering of 50 MeV π^- from various nuclei. The filled circles are results from the present experiment. The crosses are from Ref. 2 and the open squares are from Ref. 6. The statistical errors for all data are smaller than the size of the symbols. The curves are from the optical-model calculation of Siciliano *et al.* (Ref. 17).

because not enough data on these losses as a function of pion energy in the 50–0 MeV range are available. These losses are also partly compensated by similar losses in the beam monitor counter which was used for calibration. It was therefore judged satisfactory to apply corrections for these losses directly to the data. The final corrections applied were 3 ± 2 % for 50 MeV π^+, 5 ± 2 % for 50 MeV π^-, and 1 ± 0.5 % for 30 MeV π^-.

The Monte Carlo calculations for the integrated efficiency of the center-finger counter led to the following effective solid angle for stopping pions (including ~5% stopping muons which could not be distinguished from pions): $\Delta\Omega'$ (50 MeV)$=8.5\pm0.6$ msr and $\Delta\Omega'$ (30 MeV)$=9.3\pm0.7$ msr. The cross sections listed in Tables II–IV were obtained using these solid angles in Eq. (3).

IV. RESULTS AND DISCUSSION

Our measured cross sections, listed in Tables II–IV, are illustrated in Figs. 5–7, along with results of other mea-

TABLE II. Measured center-of-mass differential cross sections for 50-MeV π^+ elastic scattering (in mb/sr). The errors in parentheses are statistical only.

^{12}C		^{48}Ca		^{208}Pb	
θ	$\sigma(\theta)$	θ	$\sigma(\theta)$	θ	$\sigma(\theta)$
50.7	4.4(2)	50.2	20.3(5)	50.0	24.4(18)
60.8	2.3(1)	60.2	11.0(3)	60.1	6.4(5)
70.9	2.5(1)	70.2	10.0(4)	70.1	2.4(2)
81.0	3.4(1)	80.2	9.7(3)	80.1	4.8(3)
91.0	4.9(1)	90.2	8.9(3)	90.1	9.4(5)
101.0	5.6(1)	100.2	5.5(2)	100.1	13.7(7)
110.9	6.0(1)	110.2	4.1(2)	120.1	13.3(7)
120.8	5.7(1)	120.2	2.8(1)	130.0	13.1(6)
130.7	5.2(1)	130.2	3.7(2)	140.0	11.7(7)
140.6	4.4(1)	140.2	4.6(2)		

TABLE III. Measured center-of-mass differential cross sections for 50-MeV π^- elastic scattering (in mb/sr). The errors in parentheses are statistical only.

^{12}C		^{13}C		^{16}O		^{40}Ca		^{48}Ca		^{90}Zr		^{208}Pb			
θ	$\sigma(\theta)$	θ	$\sigma(\theta)$	θ	$\sigma(\theta)$	θ	$\sigma(\theta)$	θ	$\sigma(\theta)$	θ	$\sigma(\theta)$	θ	$\sigma(\theta)$	θ	$\sigma(\theta)$
40.6	18.9(6)	40.6	27.4(10)	40.5	29.1(7)	40.2	107.0(28)	40.2	107.6(20)	40.1	189.6(115)	40.0	351.8(157)	95.1	5.3(6)
50.7	7.1(2)	50.7	6.8(3)	50.6	9.0(3)	50.2	31.7(8)	50.2	37.4(9)	50.1	81.3(36)	45.0	175.6(75)	100.1	9.1(6)
60.8	2.5(1)	60.8	2.5(1)	60.6	3.2(1)	60.3	16.6(5)	60.2	26.1(6)	60.1	44.5(19)	50.0	137.1(49)	105.1	17.8(10)
70.9	1.7(1)	70.8	2.7(1)	70.7	3.0(1)	70.3	15.6(4)	70.2	23.7(5)	70.1	23.3(11)	55.1	76.4(34)	110.1	17.2(9)
81.0	2.8(1)	80.9	4.2(1)	80.7	4.8(2)	80.3	13.5(4)	80.2	16.4(5)	80.1	5.0(3)	60.1	37.5(17)	115.1	21.0(11)
91.0	4.0(1)	90.9	6.5(1)	90.7	6.5(2)	90.3	8.4(2)	90.2	6.7(2)	90.1	11.4(4)	65.1	35.9(16)	120.1	8.8(7)
101.0	4.7(1)	100.9	6.7(2)	100.7	6.8(2)	100.3	3.5(2)	100.2	2.3(1)	100.1	15.6(7)	70.1	46.0(17)	125.1	9.7(9)
110.9	5.5(2)	110.8	7.6(2)	110.7	6.4(2)	110.3	0.9(1)	110.2	3.2(2)	110.1	12.8(7)	75.1	45.5(17)	130.0	3.0(4)
120.8	5.0(2)	120.8	6.3(2)	120.6	4.9(2)	120.3	1.6(1)	120.2	5.9(3)	120.1	9.9(6)	80.1	32.5(14)	135.0	1.8(4)
130.7	4.3(2)	130.7	5.5(2)	130.6	3.3(2)	130.2	3.0(2)	130.2	7.6(4)	130.1	6.1(5)	85.1	11.5(9)	140.0	3.2(6)
140.6	3.8(1)	140.6	3.6(2)	140.5	2.1(2)	140.2	4.2(2)	140.2	7.2(4)	140.1	2.3(4)	90.1	8.4(6)	145.0	7.9(11)

TABLE IV. Measured center-of mass differential cross sections for 30-MeV π^- elastic scattering (in mb/sr). The errors in parentheses are statistical only.

^{12}C		^{13}C		^{16}C		^{40}Ca		^{48}Ca		^{90}Zr		^{208}Pb	
θ	$\sigma(\theta)$	θ	$\sigma(\theta)$	θ	$\sigma(\theta)$	θ	$\sigma(\theta)$	θ	$\sigma(\theta)$	θ	$\sigma(\theta)$	θ	$\sigma(\theta)$
45.6	7.2(7)	40.5	22.6(22)	50.5	8.4(3)	40.2	105.9(51)	50.2	33.0(21)	70.1	94.8(80)	40.0	842.7(652)
50.7	5.5(3)	50.6	6.8(5)	60.6	3.4(1)	50.2	34.2(16)	60.2	34.3(14)	80.1	61.8(42)	50.0	608.7(372)
70.8	1.1(1)	60.7	2.7(2)	70.6	3.1(2)	60.2	20.2(9)	70.2	42.6(18)	90.1	19.0(13)	60.0	198.4(80)
80.9	2.4(2)	70.8	2.8(2)	80.6	4.5(2)	70.2	23.3(10)	80.2	48.6(19)	100.1	7.0(11)	70.1	25.1(44)
90.9	4.1(2)	80.8	4.0(2)	90.6	7.2(2)	80.3	31.5(12)	90.2	40.3(10)	110.1	12.3(13)	80.1	38.9(39)
110.8	7.9(3)	90.8	5.4(3)	100.6	8.3(5)	90.3	35.2(13)	100.2	35.0(14)	120.1	35.5(16)	90.1	77.2(37)
120.7	10.5(3)	100.8	8.9(4)	110.6	12.9(5)	100.3	27.1(11)	110.2	17.9(9)	130.1	35.0(46)	100.1	68.8(57)
130.7	10.2(4)	110.8	10.2(5)	120.6	13.9(5)	110.2	22.2(11)	120.2	15.0(8)	140.1	34.7(36)	110.1	18.6(22)
140.6	11.4(4)	120.7	13.8(6)	130.5	11.9(6)	120.2	17.2(10)	130.2	11.4(8)			130.0	27.2(31)
		130.6	14.9(7)	140.4	13.8(6)	130.2	9.6(9)	140.1	12.5(7)			140.0	50.2(29)
		140.5	13.7(6)			140.2	4.7(9)					150.0	48.2(38)

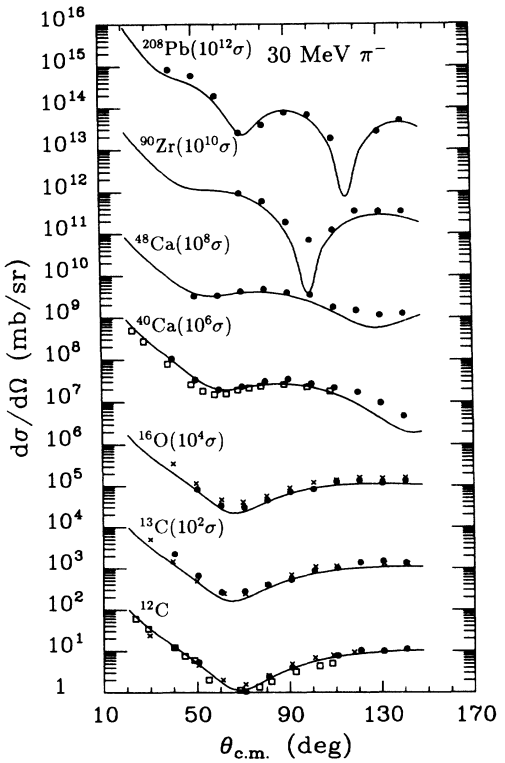

FIG. 7. Center-of-mass differential cross sections for elastic scattering of 30 MeV π^- from various nuclei. The filled circles are results from the present experiment. The crosses are from Ref. 2 and the open squares are from Ref. 7. The statistical errors for all data are smaller than the size of the symbols. The curves are from the optical-model calculations of Siciliano *et al.* (Ref. 17).

surements in the published literature. The uncertainties indicated in the tables are only statistical. The statistical error bars are in all cases too small to be visible in the figures. In addition to the statistical errors, there are systematic errors in cross sections due to uncertainties in various measured quantities. The sources and their contributions are the spectrometer angle (1%), target angle (3%), target thickness (1%), background subtraction (5%), decay muon monitor calibration (10% for 50 MeV π^+ and π^-, 20% for 30 MeV π^-), and effective solid-angle determination (8%). In quadrature these errors contribute an uncertainty of ~15% at 50 MeV and ~20% at 30 MeV.

In Fig. 5 we present our π^+ cross sections for ^{12}C, ^{48}Ca, and ^{208}Pb at 50 MeV. Several measurements of the ^{12}C cross sections exist in the literature.[1,2,4–6] Despite large disagreements in early results most recent measurements are in fairly good agreement. The cross sections from Preedom *et al.*[5] and Sobie *et al.*[6] are shown in Fig. 5. Our cross sections are approximately 10% lower than these. For ^{208}Pb only one prior measurement, due to Preedom *et al.*,[5] exists. Our data are in fair agreement. No earlier measurements for ^{48}Ca exist.

In Fig. 6 we present our results for π^- cross sections at 50 MeV. A comparison with earlier data is possible only in two cases, ^{12}C and ^{13}C. The 1978 TRIUMF cross sections of Johnson *et al.*[2] for both ^{12}C and ^{13}C are too large, as indicated by the later TRIUMF results of Sobie *et al.*[6] Our results are in good agreement with those of Sobie *et al.* at angles below 60°, and are 10–20% smaller at larger angles.

In Fig. 7 we present our results for π^- cross sections at 30 MeV. We also show the results of Johnson *et al.*[2] for ^{12}C and ^{13}C, and of Wright *et al.*[7] for ^{12}C and ^{40}Ca. The agreement between our cross sections and those of Johnson *et al.*[2] is good for ^{12}C and ^{13}C and fair for ^{16}O. However, the results of Wright for ^{12}C are about 20% smaller than ours for $\theta > 70°$. For ^{16}O they are 20–30% smaller than ours at all angles.

We have no explanation for the discrepancies mentioned above except to note that while all our measurements were made in the same setup during one experiment, the measurements by the other authors for different targets were made in different experiments, done at different times.

In the energy region, 100 MeV $\leq T(\pi) \leq 300$ MeV, the $\Delta(3,3)$ resonance plays a dominant role in pion-nucleus interactions, and the most successful development of theory has been along the lines of what is called the "delta-hole" model. At lower energies the importance of the delta is less, and most of the theoretical developments have been motivated by the zero-energy pionic-atom problem. The seminal work on low-energy pion-nucleus interactions was done by Ericson and Ericson[12] in 1966 in relation to the study of pionic atoms. It was shown that in the presence of the nuclear medium the pion-nucleon interaction is considerably modified. Short- and long-range (Pauli) correlations, medium polarization effects, and true absorption on nucleon pairs all play a part in making the effective interaction quite different from the free pion-nucleon interaction.

The work of the Ericsons was followed by the phenomenological calculations of Thies[13] and of the Michigan State University (MSU) group, Stricker, McManus, and Carr[14] and Carr, McManus, and Stricker-Bauer.[15] In the widely quoted work of the MSU group, the data for pionic atoms, low-energy π^+ elastic scattering, and $\pi^\pm$ absorption experiments on a large number of nuclei were used to obtain the best-fit values of the parameters of the pi-nucleus optical potential. The potential is[14]

$$\frac{-2\omega U}{4\pi} = p_1 b(r) + p_2 B(r) - \nabla \cdot \frac{L(r)}{1+(4\pi/3)\alpha L(r)} \nabla + \frac{1}{2}\left[1-\frac{1}{p_1}\right]\nabla^2 c(r) + \frac{1}{2}\left[1-\frac{1}{p_2}\right]\nabla^2 C(r) \tag{4}$$

plus Coulomb terms. The potential contains first-order s- and p-wave terms, $b(r)$ and $c(r)$, whose isoscalar parts are proportional to the single-particle densities $\rho(r)$ and whose isovector parts are proportional to the density differences

$$\delta\rho(r) = \rho_n(r) - \rho_p(r) .$$

The second-order s- and p-wave terms, $B(r)$ and $C(r)$, arise primarily from pion absorption. Their isoscalar parts are proportional to two-particle densities, $\rho^2(r)$, and their isovector parts are proportional to $\rho(r)\delta\rho(r)$. α is the Lorentz-Lorenz-Ericson-Ericson parameter, and p_1 and p_2 are the kinematical factors arising from the transformation from the pi-nucleon to the pi-nucleus center of mass.

Siciliano *et al.*[16] have extended the work of the MSU group by making an isospin-invariant formulation of elastic scattering, single charge exchange (SCX), and double charge exchange (DCX). The optical potential for this coupled-channel model has a natural decomposition in terms of isoscalar (U_0), isovector (U_1), and isotensor (U_2) parts. The potential is written as

$$U = U_0 + (\tau \cdot \mathbf{T})U_1 + (\tau \cdot \mathbf{T})^2 U_2 \ , \tag{5}$$

where U_0, U_1, and U_2 each have an s-wave and a p-wave part, both of which have a first-order, single-nucleon component and a second-order, two-nucleon component. The guiding principle in the fits to the data by Siciliano *et al.* is that the pionic-atom and elastic scattering data primarily determine the isoscalar potentials, the SCX data are most sensitive to the isovector components and the DCX data are most sensitive to the isotensor components. In the first step of obtaining the best-fit parameters as a function of energy, Siciliano and collaborators[17] fix the first-order parameters to those obtained from πN phase shifts, and set equal to zero all components of the isotensor potential and the second-order components of the isovector potential. They then determine the remaining parameters by fits to all the available data on pionic atoms, π^+ elastic scattering, ad π^- elastic scattering for the $N=Z$ nuclei ^{12}C, ^{16}O, and ^{40}Ca.

The isoscalar and isovector parameters of Siciliano *et al.*[16,17] have a one-to-one correspondence with those of the MSU group. As shown in Table V, the first-order parameters of Siciliano *et al.* are essentially identical to the set E parameters of the MSU search because both groups obtain them from πN phase shifts. However, the second-order isoscalar parameters B_0 and C_0 differ substantially because of the different procedures used for obtaining them from fits to the π-nucleus data. The theoretical curves shown in Figs. 5–7 are from Siciliano *et al.*[17]

As seen in Fig. 5, the theoretical results of Siciliano *et al.* for 50-MeV π^+ scattering agree almost perfectly with the measured cross sections for ^{12}C. However, there are large differences for $N \neq Z$ nuclei, ^{48}Ca, and ^{208}Pb, especially in the minima and at large angles. As is well known, the shallow minima near $\theta = 60°$ arise primarily from s- and p-wave interference. The first diffraction minima for ^{48}Ca and ^{208}Pb occur near 120° and 70°, respectively. These minima, as calculated by Siciliano *et al.*, are considerably deeper than the measured ones. A similar large discrepancy is found in fitting the minimum in the ^{90}Zr π^+ data of Preedom *et al.*[5] (not shown in Fig. 5). This suggests that the reactive part of the optical potential is not optimum. We recall that the parameters of the model were optimized by fits to the data for self-conjugate nuclei only. Thus, the observed discrepancies may require a readjustment of the reactive parts of the isovector potentials.

The curves shown in Figs. 6 and 7 for π^- scattering at 50 and 30 MeV are essentially predictions by Siciliano *et al.*[17] because they did not have any π^- scattering data for non-self-conjugate nuclei available for their search for the best-fit parameters. We note once again that the theoretical curves fit the data quite satisfactorily for light nuclei ^{12}C, ^{13}C, and ^{16}O. However, serious discrepancies begin to develop already for ^{40}Ca. The predicted diffraction minima for $A \geq 40$ are, in general, much deeper than the measured ones. They are predicted at nearly the correct angles at 30 MeV but they grow out of phase with the data for 50-MeV scattering. The effect is best seen in ^{208}Pb for which our data are most detailed.

It is not our purpose to speculate what changes in optical potentials will be required to fit the global data presented in this paper. However, it is quite clear that there are systematic differences between the nature of the

TABLE V. A-independent optical-model parameters of Siciliano *et al.* (Refs. 16 and 17) used for the theoretical predictions shown in Figs. 5–7. For comparison the best-fit parameters determined by the MSU group (Ref. 15) are also listed. Notice that the first-order parameters b_0, b_1, and c_0, c_1, determined from πN phase shifts, are essentially the same in both parameter sets. The second-order isoscalar parameters B_0 and C_0 differ.

	Siciliano *et al.*		MSU (set E)	
Parameter	50 MeV	30 MeV	50 MeV	30 MeV
b_0	$-0.071+0.006i$	$-0.056+0.003i$	$-0.061+0.006i$	$-0.055+0.002i$
b_1	$-0.124+0.000i$	$-0.122-0.000i$	$-0.13-0.002i$	$-0.13-0.001i$
B_0	$+0.146-0.045i$	$0.002+0.063i$	$-0.02+0.11i$	$-0.009+0.153i$
B_1	0	0	0	0
c_0	$0.713+0.028i$	$0.647+0.007i$	$0.70+0.028i$	$0.684+0.005i$
c_1	$0.471+0.013i$	$0.475+0.003i$	$0.46+0.013i$	$0.443+0.005i$
C_0	$0.641+0.975i$	$0.765+0.651i$	$0.36+0.54i$	$0.327+0.688i$
C_1	0	0	0	0
$\alpha_{0,1,2}$	1.6	1.6	1.4	1.4

fits for the π^+ and π^- data, and between the fits for self-conjugate nuclei and those for nuclei with $N \neq Z$. Hopefully, the use of these data in global search programs[17] will enable a better determination of all the optical-model parameters, in particular the isovector parameters. This should lead to a better understanding of the π-nucleus interaction.

ACKNOWLEDGMENTS

The authors wish to thank Dr. E. Siciliano for providing the results of his optical-model calculations prior to their publication. This work was supported in part by the U.S. Department of Energy and the Commisariat d'Energie Atomique (France).

---

*Present address: Physics Department, UCLA, Los Angeles, CA 90024.

†Present address: EG&G, Santa Barbara, CA 93106.

‡Present address: Fermi National Accelerator Laboratory, Batavia, IL 60510.

§Present address: Physics Department, Indiana University, Bloomington, IN 47405.

**Present address: Physics Department, Cornell University, Ithaca, NY 14853.

††Present address: Physics Department, University of South Carolina, Columbia, SC 29208.

‡‡Present address: Kaman Scientific, Colorado Springs, CO 80907.

§§Present address: Paul Scherrer Institute, Villigen, Switzerland.

[1]S. A. Dytman *et al.*, Phys. Rev. Lett. **38**, 1059 (1977); S. A. Dytman *et al.*, *ibid.* **39**, 53 (1977); S. A. Dytman *et al.*, Phys. Rev. C **18**, 2316 (1978).

[2]H. Dollard, K. L. Erdman, R. R. Johnson, H. R. Johnston, T. Masterson, and P. Walden, Phys. Lett. **63B**, 416 (1976); R. R. Johnson, T. G. Masterson, K. L. Erdman, A. W. Thomas, and R. H. Landau, Nucl. Phys. **A296**, 444 (1978).

[3]D. J. Malbrough *et al.*, Phys. Rev. C **17**, 1395 (1978).

[4]M. A. Moinester *et al.*, Phys. Rev. C **18**, 2678 (1978).

[5]B. M. Preedom *et al.*, Phys. Rev. C **23**, 1134 (1981).

[6]R. J. Sobie *et al.*, Phys. Rev. C **30**, 1612 (1984).

[7]D. H. Wright *et al.*, Phys. Rev. C **35**, 2258 (1987); D. H. Wright *et al.*, *ibid.* **36**, 2139 (1987); D. H. Wright, M. Blecher, B. G. Ritchie, D. Rothenberger, R. L. Burman, Z. Weinfeld, J. A. Escalante, C. S. Mishra, and C. S. Whisnant, *ibid.* **37**, 1155 (1988).

[8]A. Pevsner, J. Rainwater, R. E. Williams, and S. J. Lindenbaum, Phys. Rev. **100**, 1419 (1955); R. Williams, J. Rainwater, and A. Pevsner, *ibid.* **101**, 412 (1956); R. E. Williams, W. F. Baker, and J. Rainwater, *ibid.* **104**, 1695 (1956); W. F. Baker, J. Rainwater, and R. E. Williams, *ibid.* **112**, 1763 (1958); R. M. Edelstein, W. F. Baker, and J. Rainwater, *ibid.* **122**, 252 (1961).

[9]B. Balestri *et al.*, Nucl. Phys. **A392**, 217 (1983); G. Fournier, A. Gérard, J. Miller, J. Picard, B. Saghai, P. Vernin, P.Y. Bertin, B. Coupat, E. W. A. Lingeman, and K. K. Seth, *ibid.* **A426**, 542 (1984).

[10]E. A. Wadlinger, Nucl. Instrum. Methods **134**, 243 (1976).

[11]M. Artuso and K. K. Seth (unpublished).

[12]M. Ericson and T. E. O. Ericson, Ann. Phys. (N.Y.) **36**, 323 (1966).

[13]M. Thies, Phys. Lett. **63B**, 43 (1976); M. Thies, Phys. Lett. C **22**, 2043 (1980).

[14]K. Stricker, H. McManus, and J. A. Carr, Phys. Rev. C **19**, 929 (1979).

[15]J. A. Carr, H. McManus, and K. Stricker-Bauer, Phys. Rev. C **25**, 952 (1982).

[16]E. R. Siciliano, M. D. Cooper, M. B. Johsnon, and M. J. Leitch, Phys. Rev. C **34**, 267 (1986).

[17]E. R. Siciliano (private communication).